Overcoming the Ambient Manufacturability-Scalability-Performance Bottleneck in Colloidal Quantum Dot Photovoltaics

Ahmad R. Kirmani, Arif D. Sheikh, Muhammad R. Niazi, Md Azimul Haque, Mengxia Liu, F. Pelayo García de Arquer, Jixian Xu, Bin Sun, Oleksandr Voznyy, Nicola Gasparini, Derya Baran, Tom Wu, Edward H. Sargent, and Aram Amassian*

Colloidal quantum dot (CQD) solar cells have risen rapidly in performance; however, their low-cost fabrication under realistic ambient conditions remains elusive. This study uncovers that humid environments curtail the power conversion efficiency (PCE) of solar cells by preventing the needed oxygen doping of the hole transporter during ambient fabrication. A simple oxygen-doping step enabling ambient manufacturing irrespective of seasonal humidity variations is devised. Solar cells with PCE > 10% are printed under high humidity at industrially viable speeds. The devices use a tiny fraction of the ink typically needed and are air stable over a year. The humidity-resilient fabrication of efficient CQD solar cells breaks a long-standing compromise, which should accelerate commercialization.

As the first-generation solar cell technologies approach grid parity,[1] there is increasing need for a next-generation photovoltaic (PV) technology that can augment existing technologies by harnessing the infrared solar spectrum and also serve off-grid applications such as portable, flexible, and printable power generation at low cost. Colloidal quantum dots (CQDs) combine the benefits of solution-processability, size-tunability, and roll-to-roll

A. R. Kirmani, Prof. A. D. Sheikh,[+] M. R. Niazi, N. Gasparini,
Prof. D. Baran, Prof. A. Amassian
Physical Sciences and Engineering Division
KAUST Solar Center (KSC)
King Abdullah University of Science and Technology (KAUST)
Thuwal 23955-6900, Saudi Arabia
E-mail: aram.amassian@kaust.edu.sa
M. A. Haque, Prof. T. Wu
Physical Sciences and Engineering Division
King Abdullah University of Science and Technology (KAUST)
Thuwal 23955-6900, Saudi Arabia
M. Liu, Dr. F. P. García de Arquer, Dr. J. Xu, Dr. B. Sun, Dr. O. Voznyy,
Prof. E. H. Sargent
Department of Electrical and Computer Engineering
University of Toronto
Toronto, Ontario M5S 3G4, Canada

The ORCID identification number(s) for the author(s) of this article can be found under https://doi.org/10.1002/adma.201801661.

[+]Present address: School of Nanoscience and Technology, Shivaji University, Kolhapur 411004, Maharashtra, India

manufacturability serving as one of the most promising candidates for the next-generation PV technology.[2,3] Recent key advances including novel surface passivation protocols and efficient device designs have enabled considerable progress in CQD PV.[3–8] However, it does face two crucial challenges: "robustness" and "scalability," which have yet to be addressed without costing in device performance.[9] For these reasons, CQD solar cells fabricated under humid ambient conditions are of particular interest, as are those translated into large-area compatible, high-throughput fabrication techniques. A low-cost PV technology aiming at industrial implementation in ambient air will need to be invariant under moisture conditions during manufacture and utilization.[4,9–14] In contrast with this requirement, today's best cells—if they are to be manufactured year-round in a wide range of geographies—require careful and costly environment control during manufacture.[15] The outdoor humidity variation in major cities across the world is highlighted in **Figure 1**a in terms of absolute humidity (AH). AH and relative humidity (RH) converge in controlled temperature conditions, as RH relates to the temperature-dependent saturation level of moisture and reflects the body's ability to regulate its temperature through perspiration. Indoor humidity levels at fixed temperature therefore tend to track the outdoor AH (Figure S1, Supporting Information). Ambient air fabrication of state-of-the-art CQD solar cells performed in different humidity conditions shows that power conversion efficiency (PCE) of ≈10% is possible under AH < 5 g m^{-3} (RH < 25% at 22 °C) (Figure 1b), whereas solar cells fabricated in higher humidity conditions suffer from moderate to significant performance losses, with PCE being as low as ≈5% under AH ≈ 12 g m^{-3} (RH ≈ 60–65% at 22 °C). This makes the current generation state-of-the-art CQD solar cells unsuitable for year-round ambient manufacturing in most cities (Figure 1a) without the implementation of stringent and costly humidity controls.

A closely related challenge that remains to be addressed in the area of CQD solar cells is the translation of state-of-the-art recipes into large-area compatible coating techniques in ambient air without suffering performance losses due to upscaling and the environment. Current solid-state and
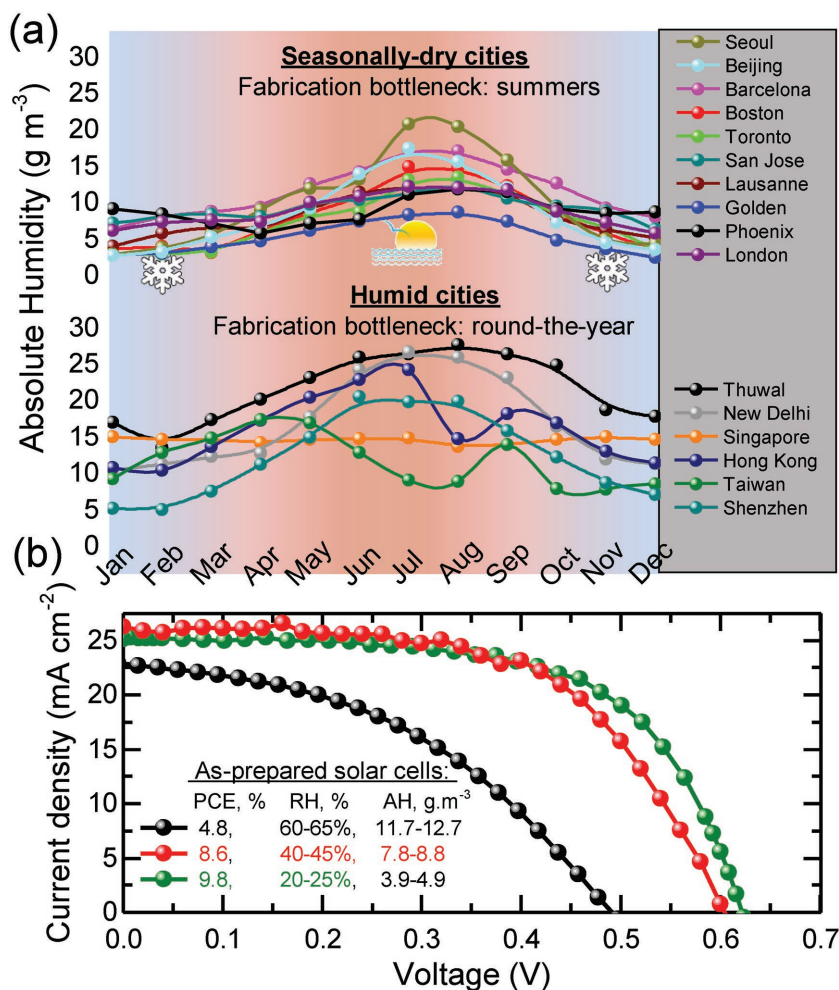
Figure 1. CQD PV in seasonally dry and humid cities. a) Absolute humidities across some of the seasonally dry cities (featuring robust CQD solar cell fabrication) and highly humid cities around the world are compared. Whereas summers are a bottleneck for device fabrication in seasonally dry cities, humid cities threaten successful device fabrication and operation almost throughout the year. b) The J–V curves of CQD solar cells freshly fabricated and tested under various RH conditions, with the lab temperature remaining the same (22 °C). High humidity severely hurts PCEs as compared to the devices made in a much drier environment.

hole transporting layer (HTL) in the humid air fabricated cells, hurting charge collection at the hole-collecting junction. We devise a strategy to compensate for deficient oxygen doping by storing the underperforming cells for a short duration in a dry air environment (0% RH) and achieve an almost 100% performance enhancement. Importantly, the improvement is irreversible and the devices are stable over a year of storage in ambient air. Next, we make use of this facile oxygen doping procedure and demonstrate >10% (8%) PCE solar cells with a blade-coated active layer on rigid (flexible) substrate at industrially relevant coating speeds of >15 m min^{-1} and extremely low materials wastage (≈4% of the CQDs normally needed). Identification, in this study, of the humidity-mediated oxygen doping has made it possible to mitigate the ill effects of humidity and develop humidity-resilient devices that will ensure the successful upscaling of low-cost CQD solar cells with minimal humidity control in different seasons, climates, and regions of the world.

The CQD solar cell architecture is schematized in **Figure 2**a. Absorber layer comprises of PbS CQDs capped with lead halide ligands (PbX$_2$, X = I, Br), obtained via SolEx.[3,18] Details of device fabrication are available in the Experimental Section (Supporting Information) and were kept the same year-round in all locations.[3] We sought to evaluate the impact of ambient conditions by carrying out SolEx and all the following device fabrication steps in humid, ambient air (≈50–65% RH, 22 °C). This humidity is representative of many humid cities (Figure 1a) and significantly higher than that in seasonally dry cities, where humidity tends to be lowest in winter months (≈10–15% RH, 22 °C) and moderately high in the summer (≈20–45% RH, 22 °C). The J–V curve for an as-prepared cell (tested immediately after fabrication) in high RH conditions is shown in Figure 2c (black curve) and corresponds to 4.8% PCE, which is nearly half of PCEs obtained immediately after low RH fabrication (Figure 1b, red and green curves). The poor result highlights how vulnerable as-fabricated CQD devices tend to be to high-humidity environments and explains why the vast majority of the high efficiency CQD solar cell results are reported from laboratories where low humidity conditions are achievable seasonally or year-round.[9,19] Higher efficiency can be achieved year-round more easily in seasonally dry cities (Figure S1b, Supporting Information), but it is still variable. Indeed, as-prepared CQD solar cells fabricated in moderately humid conditions (≈40–45% RH, 22 °C) underperformed with PCE = 8.0 ± 0.6% compared to devices fabricated in dryer ambient conditions (≈10–15% RH, 22 °C) with PCE = 9.7 ± 0.2% (Table S1, Supporting Information).

solution-phase ligand exchange (SolEx) recipes have been developed and optimized in drier ambient environments for spin coating, which typically wastes ≈90–99% of the initial ink.[3,16,17] For industrial manufacturing, spin-coating needs to be replaced with a high-throughput coating technique involving negligible materials wastage without compromising film quality or device performance, while performed in ambient air.

Herein, we tackle the dual issues currently limiting the CQD community from achieving humidity-resilient, scalable coating of devices. We begin by identifying the origin of the reduced performance in humid air-fabricated CQD solar cells.[3] We carry out all the steps—from the SolEx to solar cell fabrication—under variable moisture ambient environmental conditions. Solar cells freshly prepared in humid conditions underperform significantly, achieving nearly half the PCEs obtained using identical materials and processes in a control, low-humidity laboratory. We ascribe this effect to an unoptimally oxygen-doped CQD

ADVANCED
SCIENCE NEWS
www.advancedsciencenews.com
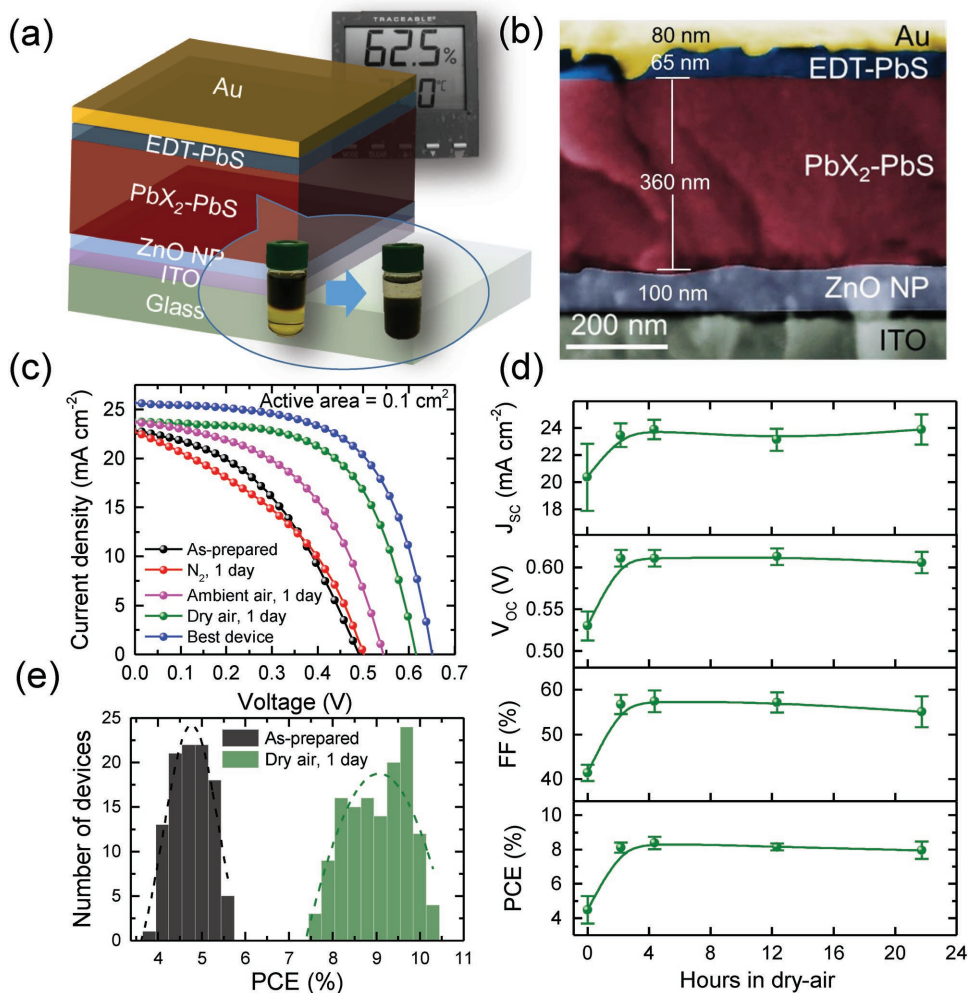
ADVANCED
MATERIALS
www.advmat.de

Figure 2. Achieving fabrication robustness. a) Schematic of the solar cell architecture. Top inset shows a typical ambient humidity value. Bottom inset is a schematic of the SolEx process. b) Cross-sectional SEM of the device showing the various layers and the corresponding thicknesses. c) J–V curves for the solar cells under various environmental conditions: as-prepared (black), stored in the nitrogen glove box for 1 d (red), stored in ambient air with ≈55–65% RH for 1 d (pink), stored in dry air with 0% RH for 1 d (green), and the best spin-coated solar cell (blue). d) Evolution of device parameters of as-prepared devices as a function of dry air-storage time. e) PCEs for the as-prepared (black) and dry air-stored (green) cells are shown as histograms. Dotted lines show the fitted Gaussians.

Inspecting the as-prepared device's figure-of-merit reveals that the short-circuit current (J_{SC}) is reasonably high, but open-circuit voltage (V_{OC}) and fill factor (FF) are well below expectations (see **Table 1**), providing the first clue into charge extraction issues. Since it is known that CQD layer fabrication in a N_2 glove box, followed by device fabrication and testing without further exposure to ambient air, also results in low PCE, we infer that oxygen doping is important.[3,4,14] We took the view that humidity interferes with the oxygen doping process of one or more of the CQD layers in the device. To test this hypothesis, we stored the as-prepared solar cells in a variety of environmental conditions, such as *N_2 glove box, humid ambient, and dry air.* The cells were re-tested after a day's storage in these conditions and the J–V curves are shown in Figure 2c. The N_2-stored cell (black) remains almost unaffected, while the humid-ambient-stored device (pink) shows a moderate enhancement in PCE largely associated with V_{OC} and FF. By contrast, the

solar cell stored in dry air (green) reaches 8.8%, nearly doubling in performance.

External quantum efficiency (EQE) spectra of the as-prepared and dry air-stored devices were compared, both at short-circuit (0 V) and maximum power-point (V_{MPP}) conditions, as shown in Figure S2 (Supporting Information). As-prepared devices show large carrier loss at V_{MPP}, which is significantly reduced upon dry air storage, confirming enhancement in carrier extraction. The shunt resistance (R_{shunt}) is found to increase substantially, which might suggest suppression of trap-assisted recombination.[20] A decrease in series resistance (R_s) can be attributed to efficient charge transport with negligible charge accumulation and recombination.[21] Upon optimization of the absorber layer thickness (≈350 nm), we achieved our best spin-coated solar cell performance of 10.2% PCE in ambient air (Figure 2c, blue), while a modification of the colloidal ink formulation (see Experimental Section in Supporting Information)

Table 1. Device parameters of solar cells exposed to various environmental conditions, averaged over 15 devices per category. PCEs shown in brackets represent best-performing devices. Lab temperature was 22 °C.

Device	RH [%]	AH [g m^{-3}]	J_{SC} [mA cm^{-2}]	V_{OC} [V]	FF [%]	PCE [%]	R_{shunt} [kΩ cm^{-2}]	R_s [Ω cm^{-2}]
As-prepared	55–65	10.7–12.7	23.1 ± 1.2	0.48 ± 0.02	41.2 ± 1.9	4.6 ± 0.4 (4.7)	0.9	5.9
N$_2$, 1 d	0	0	22.3 ± 0.7	0.50 ± 0.01	41.1 ± 1.7	4.6 ± 0.2 (4.5)	0.5	5.2
Ambient air, 1 d	55–65	10.7–12.7	23.8 ± 0.9	0.55 ± 0.01	47.7 ± 2.2	6.2 ± 0.3 (6.4)	2.0	3.4
Dry air, 1 d	0	0	24.0 ± 1.0	0.60 ± 0.01	55.4 ± 2.6	8.0 ± 0.3 (8.8)	5.4	1.8
Best cell (dry air, 1 d)	0	0	25.6	0.65	61.0	10.2	4.9	1.6

helped realize 11.0% on 0.1 cm^2 and 9.2% on 1.1 cm^2 active areas (Figure S3, Supporting Information , and **Table 2**). The stabilized devices measured for several minutes under continuous lighting (Figure S4, Supporting Information) retain ≈95% of the initial PCE.

We followed the PCE enhancement of as-prepared devices upon storage in dry air conditions more closely and found that the device parameters increased and saturated within the first few hours (Figure 2d), making this a relatively rapid process that is conveniently self-limiting with no harm to device performance upon extended storage. Figure 2e shows the performance histograms of the as-prepared (black) and the dry air-stored solar cells (green). The PCEs are found to increase from 4.7 ± 0.4% for the as-prepared cells to 8.9 ± 0.7% after a day's dry air storage measured over 100 devices. These devices were fabricated occasionally during various months. Accordingly, the RH and AH fluctuated between 55–65% and 10.7–12.7 gm^{-3} (at lab temperature of 22 °C), leading to a larger standard deviation in PCEs of dry air-stored devices (Figure 2e). These results indicate that performance of solar cells processed in high and variable humidity conditions can be recovered by briefly storing them in dry air when coating and manufacturing cannot be carried out in low and controlled humidity conditions.

An important test for CQDs aged in dry air is the irreversibility and long-term stability of the benefits of aging. We aged them in their respective environments over a period of several months. **Figure 3**a shows the PCEs after 1 d and after 1 month of fabrication, in the form of bars, with percentage PCE increase/decrease shown on top of the bars. The cell stored in N$_2$ (red bars)

is relatively stable after 1 month. The ambient-stored device (pink bars) shows an initial performance enhancement, as discussed earlier, but sees a slight drop in performance over time. Besides showing the highest PCE gains, the dry air-stored cell (green bars) is highly stable and continues to show almost 8.8% PCE at the end of 1 month of storage in dry air. Figure 3b shows the average device parameters of the dry air-stored cells over a 12 month time frame. The devices retain ≈70% of their initial performance. We transferred some of these devices, after 1 d storage in dry air, to the ambient high-humidity environment with the aim of testing long-term stability in the humid ambient. The data are shown in Figure 3b as black points and, remarkably, also exhibit high stability. These results suggest that the positive effects of a relatively brief storage period in dry air conditions are irreversible and are not lost even after re-exposure to humid air. These devices do not employ any encapsulation and are among the most stable thin film solar cells reported to date. We have gone a step further by measuring the long-term photostability of these devices, an important PV attribute largely ignored in CQD solar cells (Figure S5, Supporting Information). The data reveal an initial burn-in over a 3 h period, after which devices are remarkably stable, degrading a further ≈10% after 250 h of illumination, highlighting the remarkable photostability of CQD solar cells.

Increases in V_{OC} and FF after dry air storage hint at interfacial band alignment issues inside the as-prepared solar cell, which appear to be relieved upon dry air storage. Hence, this can be narrowed down to either the interaction of the as-cast PbX$_2$-PbS CQD absorber or the as-cast EDT-PbS CQD HTL

Table 2. Device parameters of some high-performance CQD solar cells reported to date on various active areas.

Device area [cm^{-2}]	Device parameters				Year	Reference
	J_{SC} [mA cm^{-2}]	V_{OC} [V]	FF [%]	PCE [%]		
0.01	26.5	0.54	64.0	9.2	May 2014	[4]
0.03	23.5	0.63	65.0	9.6	April 2016	[19]
0.05	23.9	0.66	68.0	10.7	October 2015	[34]
	22.3	0.64	72.0	10.2	November 2015	[35]
	22.2	0.67	69.0	10.3	May 2016	[36]
	22.8	0.65	72.0	10.6	May 2016	[37]
	24.3	0.64	69.0	10.8	April 2016	[38]
	27.2	0.61	68.0	11.3	November 2016	[3]
0.10	25.6	0.65	61.0	10.2		This work
0.10	28.8	0.66	57.8	11.0		This work
1.10	28.1	0.62	53.2	9.2		This work

ADVANCED
SCIENCE NEWS

www.advancedsciencenews.com
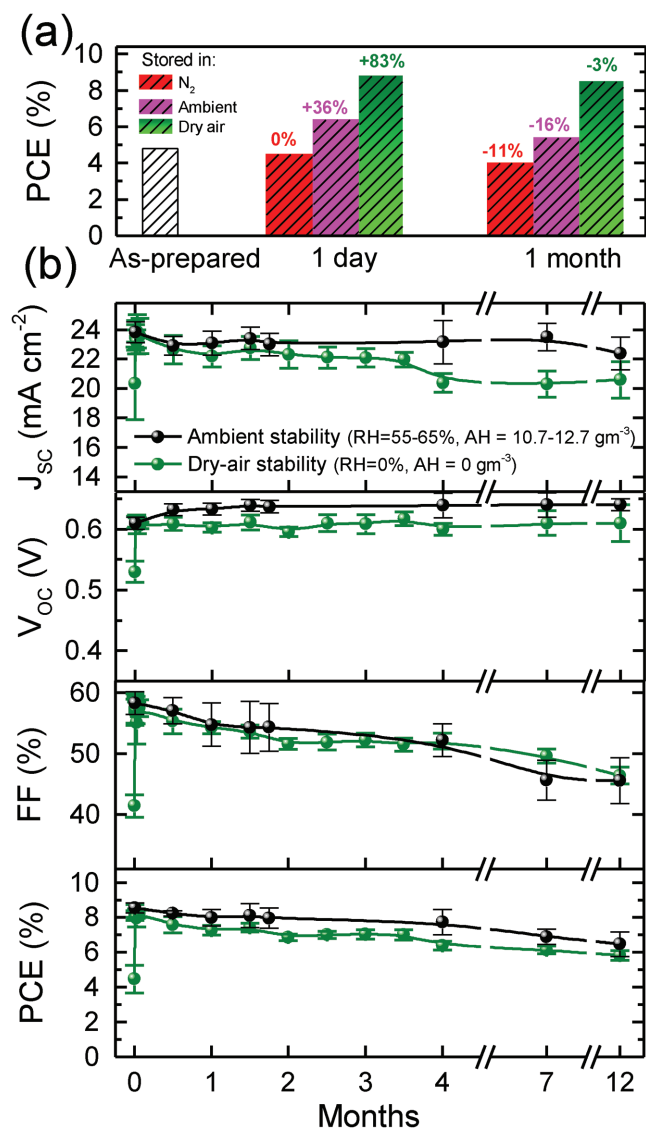
ADVANCED
MATERIALS

www.advmat.de

Figure 3. Long-term stability. a) Evolution of PCEs for solar cells corresponding to Figure 1c. N_2-soaked solar cell fails to show any PCE increase but stays stable over time. The device stored in ambient air initially shows a 36% increase in PCE, however, degrades later. However, the dry air-soaked solar cell stays considerably stable after showing a significant initial increase of >80%. b) Evolution of device parameters (J_{SC}, V_{OC}, FF, and PCE) for a set of dry air-stored devices (green). As discussed, the device parameters undergo an initial increase before achieving stability. The increase comes primarily from V_{OC} and FF. Also shown is the stability of a set of devices stored in the ambient (black). These solar cells were oxygen doped by storage in dry air for a day, before being transferred to the ambient for a year.

with the dry air environment, or possibly both. To de-convolute these possibilities, we first fabricated a control solar cell that employed a PbX_2-PbS CQD absorber layer deposited in a dry air glove box, while the CQD HTL was deposited in the humid ambient. We observed almost similar behavior in device parameters as in solar cells fabricated entirely in humid air. The V_{OC} and FF were low for the as-prepared device and increased upon dry air storage (Figure S6, Supporting Information). This

indicates the CQD absorber is immune to interactions with dry air and is unaffected by deposition in humid air. As the second control, we fabricated a solar cell where the PbX_2-PbS CQD absorber was deposited in humid ambient while the EDT-PbS CQD HTL was coated in the dry air box. Interestingly, we found a substantially high V_{OC} for the as-prepared device, along with a higher starting PCE of 6.8%. A ≈5–6 h dry air storage further increased the V_{OC} and FF leading to a final PCE of 9.3% (Figure S7, Supporting Information).

Having singled out the CQD HTL as the primary culprit for low initial PCEs when processed in humid ambient air, we probed the chemical interactions of the layers with oxygen and moisture. We employed photoemission spectroscopy, a highly surface-sensitive characterization tool to study chemical and electronic changes at interfaces.[16,22,23] The sample consisted of the PbX_2-PbS CQD absorber layer having a ≈50 nm EDT-PbS CQD HTL on top, mimicking the solar cell architecture. **Figure 4**a,b, respectively, shows the S2p and O1s core level peaks for the as-prepared film and also after a day's storage in dry air, obtained from high-resolution X-ray photoemission spectroscopy (XPS). We found that upon dry air storage, the bound EDT ligands decreased while the unbound thiolates increased, accompanied with an increase in sulfite and sulfate species. O1s peak (Figure 4b) shows formation of sulfate and sulfite with a small contribution from lead oxide (PbO).[24,25] For further details, please see Table S2 (Supporting Information) and related discussion.

These findings (please see the Supporting Information for discussion) explain that although directly exposing the as-prepared devices to the humid ambient (without the dry air storage) can lead to a partial PCE increase owing to an incomplete oxidation (pink J–V curve, Figure 2c), the adsorbed H_2O causes these devices to be unstable over time. Directly storing the as-prepared devices in dry air leads to a strong oxidation of the HTL without any H_2O adsorption on the CQD surfaces. These solar cells, therefore, lead to maximum PCE boost (green J–V curve, Figure 2c) with highest stability.

Ultraviolet photoemission spectroscopy (UPS) was employed to study the impact of oxidation on the HTL energetics (Figure S12, Supporting Information). Figure 4c shows the schematic of the respective band structures. It is found that oxidation of the CQDs in the HTL, in fact, p-dopes the HTL lowering Fermi level (E_F) by ≈0.2 eV. This is commensurate with an ≈0.2 eV shift to lower binding energy in the XPS core levels upon dry air storage. Moreover, concomitant shifts in the secondary electron cutoff and the valence band edge of equal magnitude (Figure S12, Supporting Information) refute the possibility of surface dipole formation.[26,27] Besides, suppression of valence band features around 1.5 and 3 eV upon dry air storage support oxidation of surface sulfur atoms, as previous studies have ascribed these features to S orbitals.[28,29] Field-effect transistor data point toward an increase in p-character of the EDT-PbS CQD films upon air storage (Figure S19, Supporting Information). Hole mobility is found to increase from 4.1×10^{-5} cm^2 V^{-1} s^{-1} for as-prepared films to 1.0×10^{-4} cm^2 V^{-1} s^{-1} upon air storage suggesting improved hole transport. Further, a shift of the threshold voltage (V_{th}) from −0.74 to 1.45 V is indicative of increased hole concentration, giving a further proof of oxygen doping of the HTL.

ADVANCED
SCIENCE NEWS
www.advancedsciencenews.com
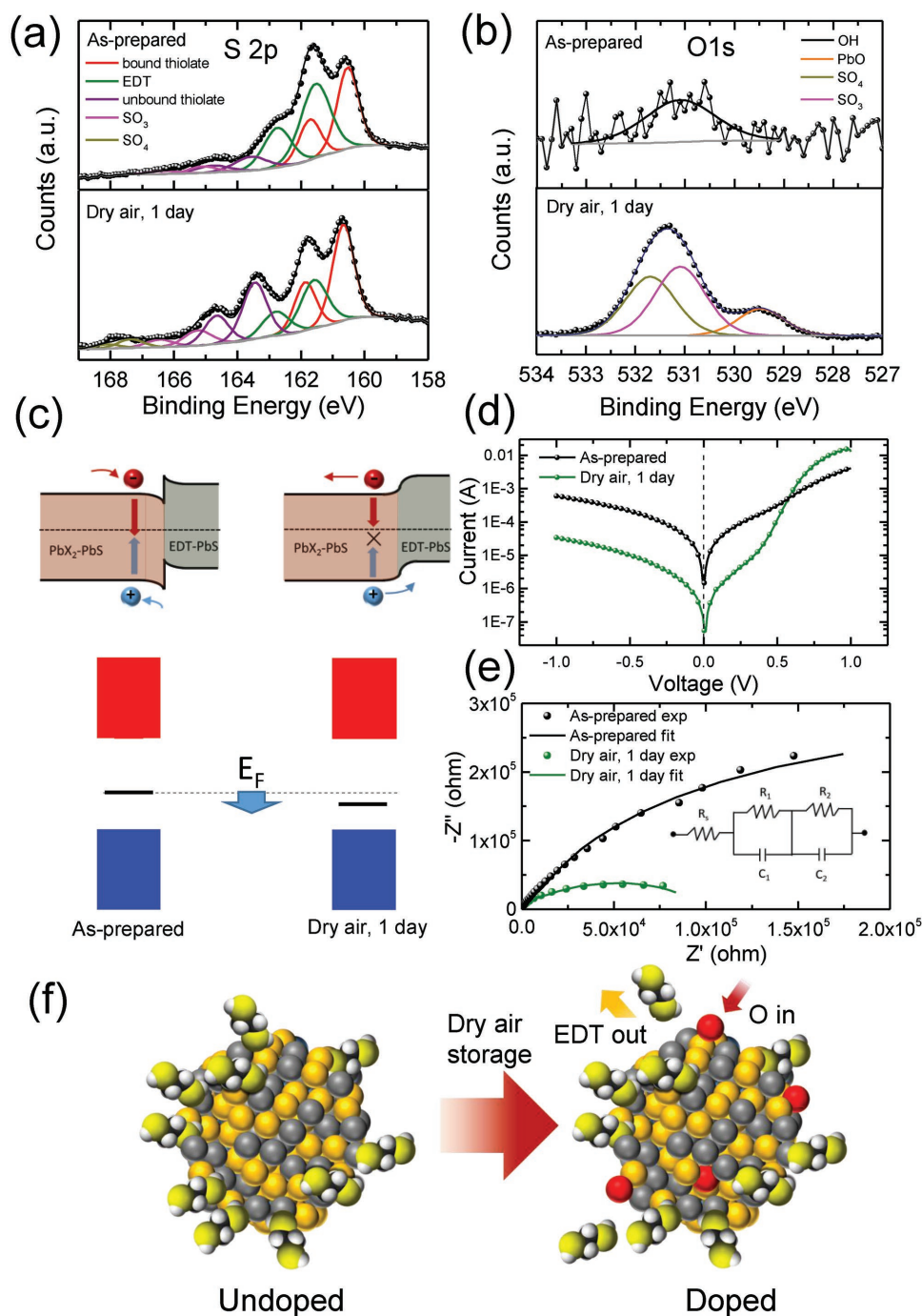
ADVANCED
MATERIALS
www.advmat.de

Figure 4. Oxygen-doping of the EDT-PbS CQD HTL. XPS data showing S2p and O1s core level peaks for the as-prepared and dry air-stored samples. The films considered for these measurements had the same architecture as the CQD stack used for solar cells (EDT-PbS CQD layer on top of a PbX_2-PbS CQD thick film). a) S2p core level peaks suggest that upon storage in dry air, QDs lose some of the EDT ligands (green components) leading to an increase in the unbound thiolate (purple components). This is, however, accompanied by an increase in oxidation species (SO_3 and SO_4) observed at higher binding energies (pink and light-green components). b) This is confirmed from the O1s peak that consists of three components belonging to $PbSO_3$, $PbSO_4$, and a small contribution from PbO. The as-prepared sample has a negligible amount of O, which might correspond to Pb-OH. c) Band structures derived from a combination of UPS and optical spectroscopy are shown for the two cases.[22,26] The Fermi level (black) is found to shift toward the valence band (blue) for the dry air-stored sample suggestive of p-doping induced by O. This leads to a scenario, shown in the inset, where oxygen dopes the EDT-PbS CQD HTL tuning band alignment at the hole-collecting interface and reducing carrier recombination. "X" in the schematic represents a reduced probability of carrier recombination at the absorber:HTL interface upon dry air storage. d) Dark J–V curves for the as-prepared cell (black) and after dry air storage (green). A significantly reduced current in the reverse bias after dry air storage implies a higher fill factor, while the S-shape in the forward bias suggests a higher V_{OC}. e) Nyquist plots of the impedance measurements for the solar cell measured in dark at 0 V bias right after preparation (black) and upon dry air storage. The fitted equivalent circuit is shown in the inset. f) Schematic describing the process of oxygen doping as discerned from experimental and theoretical insights.

ADVANCED
SCIENCE NEWS
www.advancedsciencenews.com

ADVANCED
MATERIALS
www.advmat.de

These findings suggest that the as-prepared solar cells suffer from an un-optimally doped HTL leading to band alignment issues at the hole-collecting junction, increasing interfacial carrier recombination. Dry air storage effectively p-dopes the HTL, tuning the interfacial band alignment suppressing recombination near the back end of the solar cell. As expected based on control device experiments, we find that the PbX_2-PbS CQD absorber layer is largely immune to interactions with oxygen (Table S4 and Figure S13, Supporting Information). To further substantiate our claim that the ambient moisture does, in fact, compete with atmospheric oxygen during chemical interaction with CQD surface, we simulated the scenario using density functional theory calculations. Obtained binding energies for oxygen and moisture are 0.41 and 0.48 eV, respectively, which correspond to a 16-fold difference in the bound species population at room temperature.

Dark J–V curves (Figure 4d) and impedance spectroscopy (Figure 4e) provide additional proof of enhanced charge transport upon dry air storage (please see the Supporting Information for discussion). These experimental and theoretical insights allow us to deduce the mechanism of oxygen doping shown in Figure 4f. Under this premise, atmospheric oxygen and ambient moisture compete to functionalize the EDT-PbS CQD surfaces. Due to high RH, moisture succeeds in blocking

the ingress of oxygen molecules, thereby resulting in poorly doped CQDs. Storage in a 0% RH dry box shifts the equilibrium in favor of oxygen, which diffuses through the top Au electrode and edges. Gas diffusion through metal films is a well-known phenomenon.[30–33] Oxygen replaces moisture and attaches to the CQD surface, removing some of the EDT ligands in the process, and results in optimally p-doped EDT-PbS CQDs.

The CQD PV performance achieved herein is compared with a few recent reports in Table 2. Besides having a three to ten times larger active area of 0.1 cm^2, our devices carry the obvious advantage of fabrication under a challenging high-humidity ambient environment, which more realistically reflects the conditions in many cities around the world (Figure 1).

Having overcome the challenge of ambient air fabrication, we took the aim of demonstrating scalably coated CQD solar cells under similarly high-humidity ambient conditions. We deployed high-speed blade coating (**Figure 5**a), to print the CQD absorber in a single-step under ambient conditions ($\approx$50–65% RH). Coating was done at a speed of >15 m min^{-1}, closely mimicking industrial requirements. Figure 5b shows the J–V curves for blade-coated CQD solar cells with active areas of 0.1 cm^2 (blue) and 0.5 cm^2 (green). Our blade-coated solar cells achieve performance parity with spin-coated devices (Figure 2c), while requiring $\approx$96% less CQD material. In other words, blade
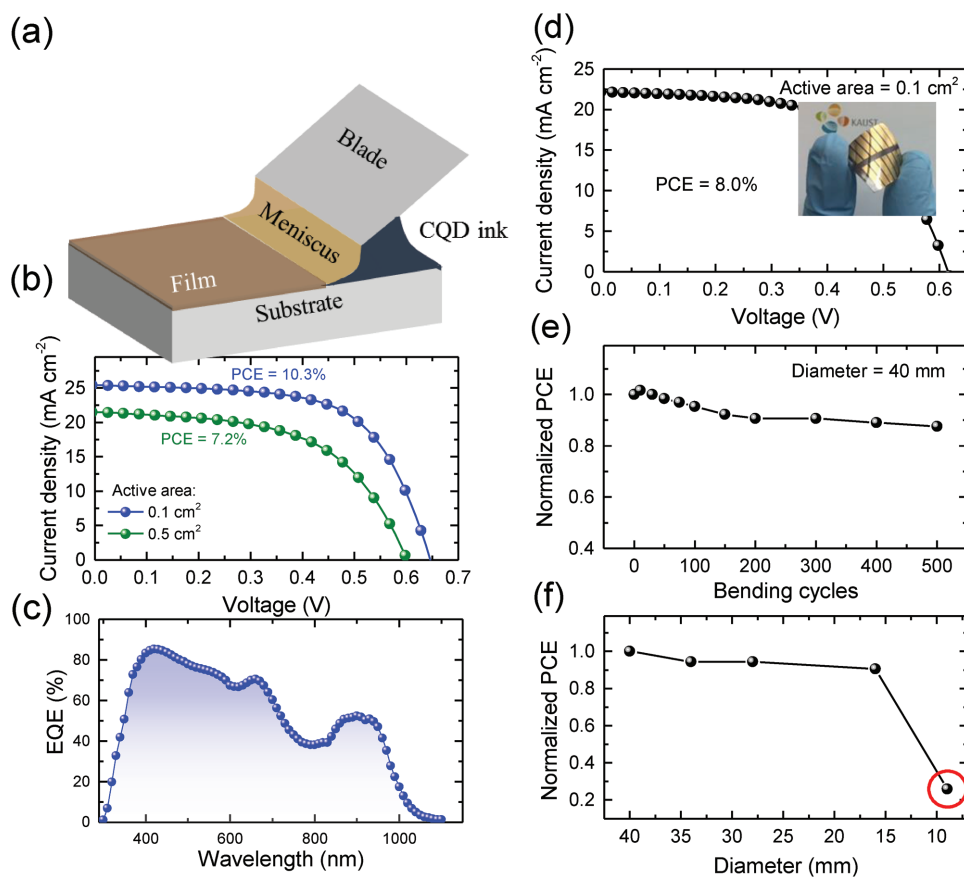

Figure 5. Blade-coated CQD solar cells. a) Schematic of the blade-coating setup employed. b) J–V curves of 0.1 cm^2 (blue) and 0.5 cm^2 (green) active area blade-coated solar cells. c) EQE spectrum of the 0.1 cm^2 active area blade-coated solar cell. d) J–V curve of the best flexible CQD solar cell fabricated via blade coating. e) Bending stability of the flexible solar cell after several bending cycles at a diameter of 40 mm, and f) for various bending diameters. Data circled in red corresponds to the failure diameter.

Table 3. Comparison of CQD solar cells fabricated via various routes.

Deposition scheme	Fabrication method	Device area [cm^2]	CQD amount required [mg cm^2]	PCE [%]	Year	Reference
65-85 LbL	Spray	0.05	15.5	8.1	November 2015	[39]
10-12 LbL	Spin	0.05	5.8	10.8	April 2016	[40]
3-LbL	Spin	0.05	3.8	6.8	June 2014	[16]
Single step	Spin	0.05	2.5	11.3	November 2016	[3]
	Blade	0.10	0.1	10.3		This work

coating allows the fabrication of ≈25 solar cells with the same amount of CQD material (by mass) needed to fabricate one spin-coated solar cell. **Table 3** compares the CQD materials consumption by some of the standard device fabrication routes and clearly suggests blade coating as a unique, high-throughput, roll-to-roll compatible CQD printing technique. A histogram of blade-coated solar cell performances (over 50 devices) is shown in Figure S15 (Supporting Information). The negligibly small J–V hysteresis of the devices is demonstrated in Figure S16 (Supporting Information). We have also fabricated cells where the CQD HTL was also prepared using a single blade-coating step and achieved a similar PCE of ≈10%, further curbing materials consumption (Figure S17, Supporting Information).

Making use of this high-throughput coating technique, we also demonstrate flexible CQD solar cells on polyethylene terephthalate (PET) substrate. Such a technology is of particular interest for niche applications such as wearable electronics, portable devices, and other in-door applications.[2,41,42] Since these applications do not demand high power input, naturally, the requirement on PCEs is relaxed while becoming stricter on mechanical bending durability. Our best flexible solar cell gives 8.0% PCE. Figure 5d–f shows the J–V curves of the best flexible device along with their associated bending stability. Figure S18 (Supporting Information) shows a histogram of flexible device performances demonstrating high reproducibility with minimal variation. **Table 4** summarizes the blade-coated solar cells fabricated on glass and PET substrates under high-humidity ambient conditions.

To sum up, we demonstrated humidity-mediated oxygen doping in CQD solar cells and used this insight to overcome two crucial challenges that currently hinder industrial scale-up of CQD PV, namely, scalable fabrication in high and variable humidity conditions, without compromising performance. Initially ≈5% PCE solar cells produced in 50–65% RH air transform into highly stable, ≈10% PCE devices upon brief storage in a dry air environment. We show that the as-prepared devices

suffer from an unoptimally doped HTL in high-humidity conditions leading to issues with charge transport across the device. Storage in dry air produces oxidation species and p-dopes the HTL relieving band misalignment leading to high-performing solar cells. Our best device of 10.2% PCE at 0.1 cm^2 active area is the highest-performing CQD solar cell fabricated under an ambient of 50–65% RH. Next, we overcome the scalability challenge demonstrating >10% solar cells via high-speed blade coating. The CQD absorber layers are prepared at blade speeds of >15 m min^{-1}, mirroring the industrial requirements, curbing ≈96% CQD materials wastage. The CQD HTL is also prepared using blade coating without noticeable loss in PCE, demonstrating a path toward fully scalable manufacturing of CQD PVs. Our study breaks a long-standing trade-off between high-moisture resilience, ambient-air scalable manufacturing, and high PCEs of the CQD PV technology, bringing it a significant step closer to industrial implementation.

Supporting Information

Supporting Information is available from the Wiley Online Library or from the author.

Acknowledgements

Conflict of Interest

The authors declare no conflict of interest.

Keywords

Table 4. Device parameters of blade-coated CQD solar cells reported in this work average over 20–30 devices per category. PCEs shown in brackets represent best-performing devices.

Substrate	Active area [cm^2]	J_{SC} [mA cm^{-2}]	V_{OC} [V]	FF [%]	PCE [%]
Glass/ITO	0.1	25.0 ± 0.7	0.63 ± 0.02	59.1 ± 2.7	9.3 ± 0.5 (10.3)
	0.5	21.6 ± 0.6	0.61 ± 0.01	53.3 ± 2.4	7.0 ± 0.2 (7.2)
PET/ITO	0.1	22.6 ± 0.5	0.58 ± 0.02	55.6 ± 1.7	7.3 ± 0.3 (8.0)

[1] A. Louwen, W. G. J. H. M. van Sark, A. P. C. Faaij, R. E. I. Schropp, *Nat. Commun.* **2016**, *7*, 13728.

[2] C. R. Kagan, E. Lifshitz, E. H. Sargent, D. V. Talapin, *Science* **2016**, *353*, aac5523.

[3] M. Liu, O. Voznyy, R. Sabatini, F. P. Garcia de Arquer, R. Munir, A. H. Balawi, X. Lan, F. Fan, G. Walters, A. R. Kirmani, S. Hoogland, F. Laquai, A. Amassian, E. H. Sargent, *Nat. Mater.* **2017**, *16*, 258.

[4] C.-H. M. Chuang, P. R. Brown, V. Bulović, M. G. Bawendi, *Nat. Mater.* **2014**, *13*, 796.

[5] J. Tang, K. W. Kemp, S. Hoogland, K. S. Jeong, H. Liu, L. Levina, M. Furukawa, X. Wang, R. Debnath, D. Cha, K. W. Chou, A. Fischer, A. Amassian, J. B. Asbury, E. H. Sargent, *Nat. Mater.* **2011**, *10*, 765.

[6] J.-S. Lee, M. V. Kovalenko, J. Huang, D. S. Chung, D. V. Talapin, *Nat. Nanotechnol.* **2011**, *6*, 348.

[7] J. Lim, Y.-S. Park, V. I. Klimov, *Nat. Mater.* **2017**, *17*, 42.

[8] K. Wu, H. Li, V. I. Klimov, *Nat. Photonics* **2018**, *12*, 105.

[9] L. Tan, P. Li, B. Sun, M. Chaker, D. Ma, *ACS Energy Lett.* **2017**, *2*, 1573.

[10] J. Zhang, J. Gao, C. P. Church, E. M. Miller, J. M. Luther, V. I. Klimov, M. C. Beard, *Nano Lett.* **2014**, *14*, 6010.

[11] M. A. Abbas, M. A. Basit, S. J. Yoon, G. J. Lee, M. D. Lee, T. J. Park, P. V. Kamat, J. H. Bang, *J. Phys. Chem. C* **2017**, *121*, 17658.

[12] H. Y. Kim, D.-E. Yoon, J. Jang, D. Lee, G.-M. Choi, J. H. Chang, J. Y. Lee, D. C. Lee, B.-S. Bae, *J. Am. Chem. Soc.* **2016**, *138*, 16478.

[13] M. H. Zarghami, Y. Liu, M. Gibbs, E. Gebremichael, C. Webster, M. Law, *ACS Nano* **2010**, *4*, 2475.

[14] P. H. Rekemeyer, S. Chang, C.-H. M. Chuang, G. W. Hwang, M. G. Bawendi, S. Gradečak, *Adv. Energy Mater.* **2016**, *6*, 1600848.

[15] R. Debnath, J. Tang, D. A. Barkhouse, X. Wang, A. G. Pattantyus-Abraham, L. Brzozowski, L. Levina, E. H. Sargent, *J. Am. Chem. Soc.* **2010**, *132*, 5952.

[16] A. R. Kirmani, G. H. Carey, M. Abdelsamie, B. Yan, D. Cha, L. R. Rollny, X. Cui, E. H. Sargent, A. Amassian, *Adv. Mater.* **2014**, *26*, 4717.

[17] Z. Yang, A. Janmohamed, X. Lan, F. P. García de Arquer, O. Voznyy, E. Yassitepe, G.-H. Kim, Z. Ning, X. Gong, R. Comin, E. H. Sargent, *Nano Lett.* **2015**, *15*, 7539.

[18] A. R. Kirmani, F. P. García de Arquer, J. Z. Fan, J. I. Khan, G. Walters, S. Hoogland, N. Wehbe, M. M. Said, S. Barlow, F. Laquai, S. R. Marder, E. H. Sargent, A. Amassian, *ACS Energy Lett.* **2017**, *2*, 1952.

[19] Y. Cao, A. Stavrinadis, T. Lasanta, D. So, G. Konstantatos, *Nat. Energy* **2016**, *1*, 16035.

[20] A. K. Rath, F. Pelayo Garcia de Arquer, A. Stavrinadis, T. Lasanta, M. Bernechea, S. L. Diedenhofen, G. Konstantatos, *Adv. Mater.* **2014**, *26*, 4741.

[21] S. Sun, T. Salim, N. Mathews, M. Duchamp, C. Boothroyd, G. Xing, T. C. Sum, Y. M. Lam, *Energy Environ. Sci.* **2014**, *7*, 399.

[22] P. R. Brown, D. Kim, R. R. Lunt, N. Zhao, M. G. Bawendi, J. C. Grossman, V. Bulović, *ACS Nano* **2014**, *8*, 5863.

[23] A. R. Kirmani, W. Peng, R. Mahfouz, A. Amassian, Y. Losovyj, H. Idriss, K. Katsiev, *Carbon* **2015**, *94*, 79.

[24] M.-J. Choi, J. Oh, J.-K. Yoo, J. Choi, D. M. Sim, Y. S. Jung, *Energy Environ. Sci.* **2014**, *7*, 3052.

[25] N. Zhao, T. P. Osedach, L.-Y. Chang, S. M. Geyer, D. Wanger, M. T. Binda, A. C. Arango, M. G. Bawendi, V. Bulovic, *ACS Nano* **2010**, *4*, 3743.

[26] A. R. Kirmani, A. Kiani, M. M. Said, O. Voznyy, N. Wehbe, G. Walters, S. Barlow, E. H. Sargent, S. R. Marder, A. Amassian, *ACS Energy Lett.* **2016**, *1*, 922.

[27] A. Tarasov, S. Zhang, M.-Y. Tsai, P. M. Campbell, S. Graham, S. Barlow, S. R. Marder, E. M. Vogel, *Adv. Mater.* **2015**, *27*, 1175.

[28] K. Katsiev, A. H. Ip, A. Fischer, I. Tanabe, X. Zhang, A. R. Kirmani, O. Voznyy, L. R. Rollny, K. W. Chou, S. M. Thon, G. H. Carey, X. Cui, A. Amassian, P. Dowben, E. H. Sargent, O. M. Bakr, *Adv. Mater.* **2014**, *26*, 937.

[29] T. Ollonqvist, T. Kaurila, M. Isokallio, M. Punkkinen, J. Väyrynen, *J. Electron Spectrosc. Relat. Phenom.* **1995**, *76*, 729.

[30] C. J. R. Smithells, C. E. Ransley, *Proc. R. Soc. LondonA* **1935**, *150*, 172.

[31] C. Bei, R. Jha, H. Lazar, N. Biswas, L. Jaehoon, L. Bongmook, L. Wielunski, E. Garfunkel, V. Misra, *IEEE Electron Device Lett.* **2006**, *27*, 228.

[32] T. S. Glen, N. W. Scarratt, H. Yi, A. Iraqi, T. Wang, J. Kingsley, A. R. Buckley, D. G. Lidzey, A. M. Donald, *Sol. Energy Mater. Sol. Cells* **2015**, *140*, 25.

[33] F. Ali, A. Sharma, J. P. Tiwari, S. Chand, *AIP Adv.* **2015**, *5*, 027108.

[34] G.-H. Kim, F. P. García de Arquer, Y. J. Yoon, X. Lan, M. Liu, O. Voznyy, Z. Yang, F. Fan, A. H. Ip, P. Kanjanaboos, S. Hoogland, J. Y. Kim, E. H. Sargent, *Nano Lett.* **2015**, *15*, 7691.

[35] X. Lan, O. Voznyy, A. Kiani, F. P. García de Arquer, A. S. Abbas, G.-H. Kim, M. Liu, Z. Yang, G. Walters, J. Xu, M. Yuan, Z. Ning, F. Fan, P. Kanjanaboos, I. Kramer, D. Zhitomirsky, P. Lee, A. Perelgut, S. Hoogland, E. H. Sargent, *Adv. Mater.* **2016**, *28*, 299.

[36] R. Azmi, S.-H. Oh, S.-Y. Jang, *ACS Energy Lett.* **2016**, *1*, 100.

[37] Z. Jin, M. Yuan, H. Li, H. Yang, Q. Zhou, H. Liu, X. Lan, M. Liu, J. Wang, E. H. Sargent, Y. Li, *Adv. Funct. Mater.* **2016**, *26*, 5284.

[38] M. Liu, F. P. de Arquer, Y. Li, X. Lan, G. H. Kim, O. Voznyy, L. K. Jagadamma, A. S. Abbas, S. Hoogland, Z. Lu, J. Y. Kim, A. Amassian, E. H. Sargent, *Adv. Mater.* **2016**, *28*, 4142.

[39] I. J. Kramer, J. C. Minor, G. Moreno-Bautista, L. Rollny, P. Kanjanaboos, D. Kopilovic, S. M. Thon, G. H. Carey, K. W. Chou, D. Zhitomirsky, A. Amassian, E. H. Sargent, *Adv. Mater.* **2015**, *27*, 116.

[40] M. Liu, F. P. G. de Arquer, Y. Li, X. Lan, G.-H. Kim, O. Voznyy, L. K. Jagadamma, A. S. Abbas, S. Hoogland, Z. Lu, J. Y. Kim, A. Amassian, E. H. Sargent, *Adv. Mater.* **2016**, *28*, 4142.

[41] X. Zhang, J. Zhang, J. Liu, E. M. J. Johansson, *Nanoscale* **2015**, *7*, 11520.

[42] I. J. Kramer, G. Moreno-Bautista, J. C. Minor, D. Kopilovic, E. H. Sargent, *App. Phys. Lett.* **2014**, *105*, 163902.